A Magnetic Network Approach to the Transient Analysis of Synchronous Machines

M. Andriollo, T. Bertoncelli, A. Di Gerlando

Department of Electrical Engineering - Politecnico di Milano
20133 Milano - Piazza Leonardo da Vinci, 32 - Italy
phone:+39 02 2399 37[07,22]; e-mail: [mauro.andriollo, tiziana.bertoncelli, antonino.digerlando]@polimi.it

***Abstract* – The technique for the simulation of the dynamic behaviour of rotating machines presented in the paper is based on an equivalent circuit representation of the magnetic configuration. The circuit parameters are obtained by a preliminary automated sequence of magnetostatic FEM analyses and take into account the local magnetic saturations.**

The adopted solution technique is based on an invariant network topology approach: its application, here presented for the operation analysis of a low-power synchronous generator, allows a great reduction of the calculation time in comparison with a commercial FEM code for the transient simulation.

1. Introduction

Since many years the most commonly used tool in advanced design and study of electromagnetic devices has been represented by the electromagnetic FEM analysis [1]-[6]. More recent implementations of FEM-based codes allow the transient simulation, taking into account the dependence on time of both the sources and the geometrical configuration. Nevertheless, the steep application of such codes does not allow a deep insight in the electromagnetic behaviour and generally results in high calculation times, even if a single configuration has to be analysed under various operative conditions. Getting worse, the performance assessment in consideration of parametric variations is time-consuming in proportion to the number of configurations to be examined.

Low-power synchronous generators emphasize such problems, due to the relevant "cross-coupling" effect between the d and q axes m.m.f.s caused by the high local saturation in the pole shoe zone.

The alternative approach, presented in this paper, is based on the representation of the synchronous machines by an equivalent magnetic circuit [8], whose various elements accurately characterise the behaviour of different zones by suitable magnetic permeances (reluctances) and m.m.f.s. Such method, implemented in a code, allows the fast and accurate calculation of the winding flux linkages, given the rotor position and the winding currents.

An effective procedure for the transient analysis was then obtained, integrating such code in a step-by-step procedure for the numerical integration of the voltage differential equations. Several integration techniques were considered, and their performances from the numerical viewpoint were investigated.

In the examples of application, the results obtained by the code based on the proposed technique are compared with the ones related to a commercial FEM code for the electromagnetic transient analysis [9].

2. Determination of the flux linkages

To illustrate and test the method, a 2D typical configuration is considered (Fig.1a), related to a 2-poles 3-phase synchronous generator with 24 stator slots, with single-layer windings. It exhibits all the local saturation phenomena, particularly relevant in the low power machines; in order to evidence the cogging effects due to the stator teeth, an open slot configuration was considered, even if it is not used in actual machines. Various circuit patterns were examined, related to different geometrical subdivisions; a good agreement with the results of the corresponding FEM analyses was obtained by the circuit representation of Fig.1b, related to the partition of Fig.1a [8]. The nodes s_i, c_i (i=0,…, n_s–1 with n_s= 24 number of stator slots) and r_j (j=0,…, n_r–1 with n_r=8 divisions of the rotor surface) identify respectively stator teeth, stator yoke radial sections and rotor boundaries (configuration symmetry was deliberately ignored, to demonstrate the procedure applicability also to unsymmetrical structures).

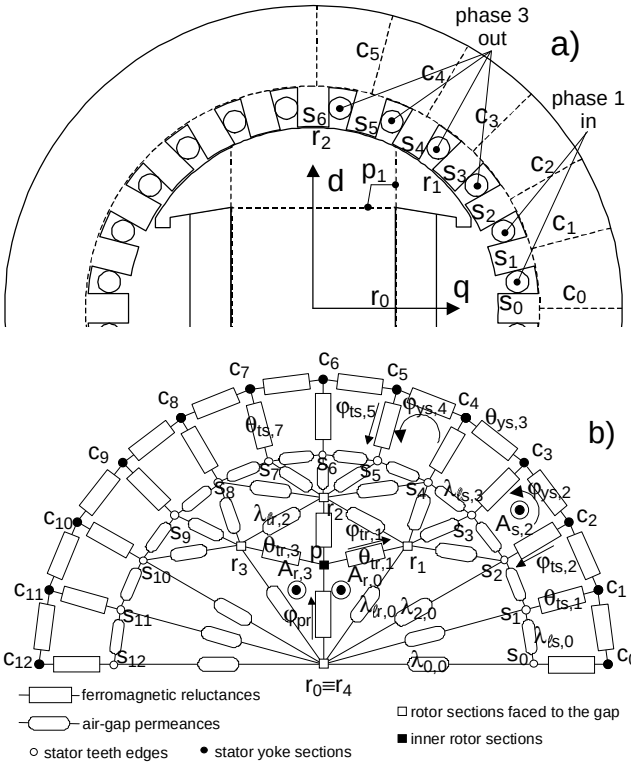

Fig.1. Synchronous machine structure and model: a): machine structure considered for the analysis (dashed lines: boundaries of the ferromagnetic branches); b): equivalent magnetic network (only some representative elements are shown and labelled).

Parameters of the magnetic circuit

The configuration is subdivided in different magnetic zones, which permeance (or reluctance) is represented alternatively as:
- a linear parameter, unaffected by the load condition but generally dependent on the stator-rotor relative position, for the magnetic paths in air (air-gap and leakage);
- a flux-dependent parameter, for paths mainly developing inside ferromagnetic branches, and therefore approximately restricted in a time-independent geometrical structure, but affected by the magnetic saturation.

The air-gap permeances are distinguished in "mutual" air-gap permeances $\lambda_{i,j}$ (i.e., related to the fluxes flowing between the *i*-th stator tooth edge and the *j*-th rotor boundary edge) and air-gap leakage permeances $\lambda_{\ell s,i}$ and $\lambda_{\ell r,j}$ (associated to the fluxes between *i*-th and (*i*+1)-th stator teeth and between *j*-th and (*j*+1)-th rotor boundaries, respectively). An automated sequence of FEM analyses allows to calculate the air-gap permeances as the ratio between the fluxes (flowing between the involved zone and the adjacent ferromagnetic surfaces) and the difference of the magnetic potential impressed by means of suitable probe sources (an infinite magnetic permeability μ_{Fe} of the iron core being provisionally assumed). The interpolation of the results obtained by such analyses sequences allows to define the various permeances as functions of the rotor position α (Fig.2a).
According to such scheme, each stator tooth is ideally coupled with each rotor zone and vice versa for every position α (in practice, the related permeance function rapidly decays as the distance between the two zones increases). Hence, the network structure, albeit non-planar, is time-invariant, the dependence on α being assigned to the permeance values: this choice greatly simplifies the analysis, because no topological update is needed during rotation.

Also the iron core reluctances are evaluated via a suitable sequence of automated FEM analyses [8]:
- the flux φ in each considered branch is evaluated by a non–linear FEA, applying suited probe m.m.f. sources, taking into account the proper non-linear $B(H)$ relationship for that ferromagnetic branch and assuming $\mu_{Fe}\rightarrow\infty$ in the rest of the iron core;
- the air-gap magnetic voltage drop (m.v.d.) can be determined evaluating the corresponding air-gap permeance, as previously explained;
- deducting the air-gap m.v.d. contribution from the total m.v.d., the drop in the ferromagnetic branch and the corresponding reluctance θ is calculated;
- the previous steps are repeated for different values of the probe m.m.f. sources;
- the interpolation of $\{\theta,\varphi\}$ values gives the non-linear function $\theta(\varphi)$ (Fig.2b).

Non-linear magnetic circuit solution algorithm

While some solvers were previously developed, just for the analysis of no-load conditions [10], the following described method leads to direct and general formulations; its integration in an efficient code for transient analysis allows good performances from the point of view of both the accuracy and speed of calculation. The solution of the magnetic network is based on explicit recursive formulations of the magnetic potentials of the nodes s_i, c_i and subsequent expressions of the fluxes on iron core branches.

Referring to the circuit of Fig.1-b, let introduce some further magnetic stator and rotor quantities:
$U_{s,i}$: magnetic potential of the *i*-th stator tooth head;
$\varphi_{ts,i}$: flux flowing out the *i*-th stator tooth;
$\varphi_{ys,i}$: flux flowing through the stator yoke section between the *i*-th and the (*i*+1)-th teeth;
$A_{s,i}$: ampere·turns in the *i*-th stator slot (between the *i*-th and the (*i*+1)-th teeth);
$U_{r,j}$: magnetic potential of the *j*-th rotor zone surface;
$\varphi_{tr,j}$: flux flowing out the *j*-th rotor zone;
φ_{pr}: flux flowing through the rotor pole;
$A_{r,j}$: ampere·turns related to rotor lap embraced by the *j*-th and the (*j*+1)-th zone.

A. Calculation of the scalar magnetic potentials

– *Stator*

Referring to the generic lap of the i-th stator slot, the following n_s recursive equations hold (i=0, 1,…, n_s–1; $\overline{i+1}$ is the remainder of the division of i+1 by n_s, so that when $i = n_s$–1, $\overline{i+1}$= 0; similarly, for i = 0, $\overline{i-1}$= n_s–1):

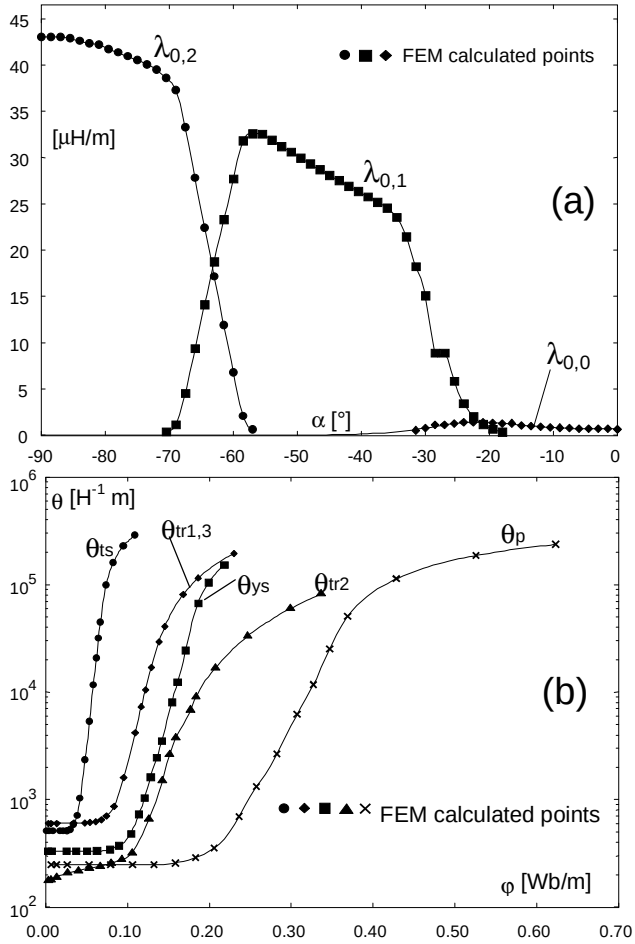

Fig.2: (a) · air-gap permeances as functions of the rotor position α; (b) - iron core reluctances as functions of the proper branch fluxes (θ_{ts}: stator teeth; θ_{ys}: stator yoke sections; $\theta_{tr1,3}$: polar shoe expansions; θ_p: polar bodies).

$$U_{s,\overline{i+1}} - U_{s,i} = A^*_{s,i}, \quad \text{with} \tag{1}$$

$$A^*_{s,i} = A_{s,i} - \theta_{ts,\overline{i+1}}\varphi_{ts,\overline{i+1}} - \theta_{ys,i}\varphi_{ys,i} + \theta_{ts,i}\varphi_{ts,i} \tag{2}$$

The terms $A^*_{s,i}$ represent the slot ampere·turns lessen by magnetic potential drops due to teeth and yoke reluctances. The fluxes conservation implies that:

$$\varphi_{ts,i} = \varphi_{ys,\overline{i-1}} - \varphi_{ys,i} \tag{3}$$

To solve the set of eqns. (1) the further eq. is introduced:

$$\sum_{i=0}^{n_s-1} \lambda_{s,i} U_{s,i} = 0 \tag{4}$$

($\lambda_{s,i} = \sum_{j=0}^{n_r-1} \lambda_{i,j}$ is the i-th stator tooth gap permeance).

and the following relation is obtained:

$$U_{s,0} = -\sum_{i=1}^{n_s-1} \lambda_{s,i} F^*_{s,i-1} \Big/ \sum_{i=0}^{n_s-1} \lambda_{s,i} = -\frac{\sum_{i=1}^{n_s-1} \lambda_{s,i} F^*_{s,i-1}}{\Lambda_{s,r}} \tag{5}$$

with $F^*_{s,i} = \sum_{h=0}^{i} A^*_{s,h}$ and $\Lambda_{s,r} = \sum_{i=0}^{n_s-1} \lambda_{s,i} = \sum_{i=0}^{n_s-1} \sum_{j=0}^{n_r-1} \lambda_{i,j}$ ($\Lambda_{s,r}$ is the global permeance between stator and rotor).

By means of (5), the other potentials $U_{s,i}$ are determined by the recursive relations (1).

– *Rotor*

Referring to Fig.1b, a sequence of rotor magnetic laps analogous to the stator ones can be recognised, and a set of n_r–1 recursive equations like (1) could be therefore obtained. Taking advantage of the geometrical and magnetic symmetry, the problem is simplified, since only $n_r/2$ equations are required, corresponding to contiguous rotor laps embracing a 180° arc (it results $U_{r,j+nr/2} = -U_{r,j}$). Defining the quantities related to the rotor ampere·turns:

$$\begin{aligned} A^*_{r,0} &= A_{r,0} + \theta_{tr,1}\varphi_{tr,1} + \theta_p \varphi_{pr} \\ A^*_{r,1} &= A_{r,1} + \theta_{tr,2}\varphi_{tr,2} - \theta_{tr,1}\varphi_{tr,1} \\ A^*_{r,2} &= A_{r,2} + \theta_{tr,3}\varphi_{tr,3} - \theta_{tr,2}\varphi_{tr,2} \\ A^*_{r,3} &= A_{r,3} - \theta_p \varphi_{pr} - \theta_{tr,3}\varphi_{tr,3} \end{aligned} \tag{6}$$

the following equations are obtained:

$$\begin{aligned} U_{r,0} &= F^*_{r,3}/2 = \left(A^*_{r,0} + A^*_{r,1} + A^*_{r,2} + A^*_{r,3}\right)/2 \\ U_{r,1} &= U_{r,0} - F^*_{r,0} \\ U_{r,2} &= U_{r,0} - F^*_{r,1} \\ U_{r,3} &= U_{r,0} - F^*_{r,2} \end{aligned} \tag{7}$$

with $F^*_{r,j} = \sum_{k=0}^{i} A^*_{r,k}$.

B. Calculation of fluxes

– *Stator*

Once the stator and rotor potentials are defined, the flux delivered by the generic i-th stator tooth is given by:

$$\begin{aligned} \varphi_{ts,i} = &-\lambda_{ts,\overline{i-1}} U_{s,\overline{i-1}} + \lambda^*_{s,i} U_{s,i} - \\ &-\lambda_{ts,i} U_{s,\overline{i+1}} - \sum_{j=0}^{n_r-1} \lambda_{ij} U_{r,j} \end{aligned} \tag{8}$$

($\lambda^*_{s,i} = \lambda_{s,i} + \lambda_{ts,i} + \lambda_{ts,\overline{i-1}}$ = i-th tooth total gap permeance).

Rearranging (3), the stator yoke fluxes can be explicited as in the following:

$$\begin{aligned} \varphi_{ys,1} &= -\psi_{s,1} + \varphi_{ys,0} \\ \varphi_{ys,2} &= -\psi_{s,2} + \varphi_{ys,0} \\ &\vdots \\ \varphi_{ys,n_s-1} &= -\psi_{s,n_s-1} + \varphi_{ys,0} \end{aligned} \tag{9}$$

with $\psi_{s,i} = \sum_{h=1}^{i} \varphi_{ts,h}$.

Since the net m.m.f. acting inside the stator yoke is null, the sum of the m. v. drops along the yoke must be zero, i.e.:

$$\sum_{i=0}^{n_s-1} \theta_{ys,i}\varphi_{ys,i} = 0 \tag{10}$$

Combining (9) and (10), $\varphi_{ys,0}$ can be expressed as:

$$\varphi_{ys,0} = \sum_{i=1}^{n_s-1} \theta_{ys,i}\psi_{s,i} \Big/ \sum_{i=1}^{n_s-1} \theta_{ys,i} \tag{11}$$

and so all the other stator yoke fluxes can be determined.

– *Rotor*

The flux in the j-th rotor zone can be expressed as a function of the magnetic potentials in the form:

$$\begin{aligned} \varphi_{tr,j} = &-\lambda_{tr,\overline{j-1}} U_{r,\overline{j-1}} + \lambda^*_{r,j} U_{r,j} - \\ &-\lambda_{tr,j} U_{r,\overline{j+1}} - \sum_{i=0}^{n_s-1} \lambda_{ij} U_{s,i} \end{aligned} \tag{12}$$

($\lambda^*_{r,j} = \lambda_{r,j} + \lambda_{tr,j} + \lambda_{tr,\overline{j-1}}$: j-th zone gap permeance).

The rotor pole flux φ_{pr} is then given by:

$$\varphi_{pr} = \varphi_{tr,1} + \varphi_{tr,2} + \varphi_{tr,3} \tag{13}$$

The previous equations define a non–linear system, requiring an iterative procedure to be solved. In such application a fixed-point technique is adopted: let $\underline{X}_{(n)}$ the set of values of the magnetic circuit quantities (ampere-turns, magnetic potentials, fluxes) evaluated at the n-th step. Entering such values in the previous equations, a preliminary updated set $\underline{X}^u_{(n+1)}$ is obtained; the new solution vector $\underline{X}_{(n+1)}$ is then determined as:

$$\underline{X}_{(n+1)} = \beta \underline{X}^u_{(n+1)} + (1-\beta)\underline{X}^u_{(n+1)} \quad . \tag{14}$$

A suited choice of the relaxation factor $\beta<1$ is essential to prevent the numerical instability, limiting at the same time the number of iterations: the higher the saturation, the lower is the instability threshold value of β. The convergence estimation is based on the calculation of the flux variation $\Delta\varphi_{(n)}$ from the n–1-th to the n-th iteration (sub-subscripts $_{(n\text{-}1)}$ and $_{(n)}$):

$$\Delta\varphi_{(n)} = \frac{\sum_{i=0}^{n_s-1}\left(\underset{(n)}{\varphi_{ts,i}} - \underset{(n-1)}{\varphi_{ts,i}}\right)^2 + \sum_{j=0}^{n_r-1}\left(\underset{(n)}{\varphi_{tr,j}} - \underset{(n-1)}{\varphi_{tr,j}}\right)^2}{\sum_{i=0}^{n_s-1}\underset{(n)}{\varphi_{ts,i}^2} + \sum_{j=0}^{n_r-1}\underset{(n)}{\varphi_{tr,j}^2}} \quad (15)$$

The iterations are continued until the number n exceeds a maximum n_{max} or $\Delta\varphi_{(n)}$ goes below a threshold value ε_φ. The process is outlined by the flow diagram of Fig.3.

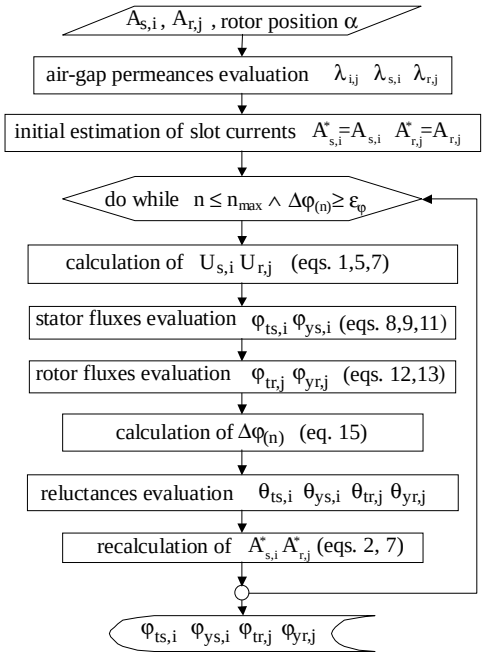

Fig.3. Outline of the procedure for the fluxes calculation.

C. Determination of the flux linkages

The stator windings flux linkages ψ_1, ψ_2, ψ_3 are determined multiplying the fluxes $\varphi_{ts,i}$ by the linkage coefficients $\{w_{p,0},\ldots,w_{p,n_s-1}\}$ of the *p*-th phase winding, according to the following formulations:

$$\psi_p = \sum_{i=0}^{n_s-1} w_{p,i}\varphi_{ts,i} \quad \text{with } p = 1,2,3$$

$$w_{p,i} = w'_{p,i-1} - \frac{1}{n_s}\sum_{i=0}^{n_s-1} w'_{p,i} \quad ; \quad (16)$$

$$w'_{p,0} = 0,\ w'_{p,i+1} = w'_{p,i} + \gamma_{p,i} \quad \text{with } i = 0,\ldots,n_s-2$$

the *p*-th phase connection coefficients $\gamma_{p,i}$ are given by the number of conductors in the *i*-th slot with a leading + if current flows towards the reader, – if it flows in the opposite direction, 0 if *p*-th phase has no conductor in the slot.
For a symmetrical 3-phase winding, once the phase 1 linkage coefficients are determined, the corresponding ones for phase 2 and phase 3 are simply obtained by shifting the coefficients to the left of $n_s/3$ and $2n_s/3$ positions respectively.

Analogous expressions can be defined for the rotor windings. More directly, the flux linkage of the N_e turns excitation winding is given by:

$$\psi_e = -N_e\left(\varphi_{tr,1} + \varphi_{tr,2} + \varphi_{tr,3}\right) \quad . \quad (17)$$

3. Procedure for the transient analysis

With reference to Fig.4, let $\underline{v}=\{v_1-v_0, v_2-v_0, v_3-v_0, v_e\}$, $\underline{i}=\{i_1,i_2,i_3,i_e\}$, $\underline{\psi}=\{\psi_1,\psi_2,\psi_3,\psi_e\}$ the voltage, current and flux vectors, respectively (*e*-subscripted quantities refer to the excitation winding, the other elements to the armature phases). The voltage equations can be expressed (according to the active bipole representation) in the matrix form:

$$\underline{v} = -\frac{d\underline{\psi}}{dt} - \underline{R}_w \cdot \underline{i}$$
$$v_p - v_0 = R_l i_p + L_l \frac{di_p}{dt} \quad (p = 1,2,3),\ v_e = -V_e \quad (18)$$

with $\underline{R}_w$ diagonal matrix related to the winding resistances $\{R_a, R_a, R_a, R_e\}$ and V_e field supply constant voltage.
The wye midpoint voltage v_0 can be determined according to the characteristics of the neutral connection: if such connection, as in most cases, is absent (i.e., $i_1+i_2+i_3=0$), the sum of the armature windings equations gives:

$$v_0 = p\left(\frac{\psi_1+\psi_2+\psi_3}{3}\right) = p\psi_0 \quad (19)$$

with ψ_0 homopolar component of the flux.

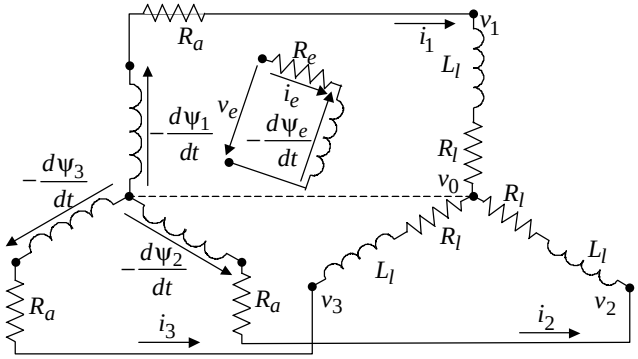

Fig.4: circuit representation of the armature and excitation windings (R_a: armature phase resistance; R_l, L_l: load resistance and inductance; R_e: excitation winding resistance).

According to (19), (18) can be rearranged as:

$$v_p = R_l i_p + L_l \frac{di_p}{dt} = -\frac{d}{dt}\left(\psi_p - \psi_0\right) - R_a i_p \quad p = 1,2,3$$
$$v_e = -V_e = -\frac{d\psi_e}{dt} - R_e i_e \quad . \quad (20)$$

Defining the equivalent global flux linkages $\phi_p=\psi_p-\psi_0+L_l i_p$ and including the armature winding resistances in the resistance diagonal matrix $\underline{R}$ with non-null elements $\{R_a+R_l, R_a+R_l, R_a+R_l, R_e\}$, (20) are rearranged as:

$$\underline{u} = \frac{d\underline{\phi}}{dt} + \underline{R}\cdot\underline{i} \quad \text{with:}$$
$$\underline{u} = \{0,0,0,V_e\},\ \ \underline{\phi} = \{\phi_1,\phi_2,\phi_3,\psi_e\} \quad (21)$$

Integrating (21) from t_k to $t_{k+1}=t_k+\Delta t$ (Δt=const) by the trapezoidal rule yields ($_k$, $_{k+1}$ subscripts refer to t_k, t_{k+1}, respectively; $\alpha_{k+1}-\alpha_k = \omega\cdot\Delta t$, with ω rotation speed):

$$\frac{\underline{u}_{k+1}+\underline{u}_k}{2}\Delta t = \underline{R}\cdot\frac{\underline{i}_{k+1}+\underline{i}_k}{2}\Delta t + (\underline{\phi}_{k+1} - \underline{\phi}_k) \quad (22)$$

Evidencing the occurring $k+1$-th state quantities $\underline{i}_{k+1}$, $\underline{\phi}_{k+1}$, it results:

$$\underline{i}_{k+1} + \frac{2}{\Delta t}\underline{R}^{-1}\cdot\underline{\phi}_{k+1} = \underline{R}^{-1}\cdot\frac{\underline{u}_{k+1}+\underline{u}_k}{2} - \underline{i}_k + \frac{2}{\Delta t}\underline{R}^{-1}\cdot\underline{\phi}_k \quad (23)$$

where all the right-side quantities are known, as soon as the previous k-th state is determined. Due to the non-linear dependence of $\underline{\phi}_{k+1}$ on $\underline{i}_{k+1}$, (23) has to be solved via an iterative algorithm, according to the following points ($^{(q)}$, $^{(q-1)}$ superscripts denote the values related to the current q-th iteration and to the previous one respectively):

- the flux $\underline{\phi}_{k+1}{}^{(q)}$ can be expressed by its Taylor series expansion arrested to the first-order term, starting from the previous estimated values $\{\underline{\phi}_{k+1}{}^{(q-1)}, \underline{i}_{k+1}{}^{(q-1)}\}$:

$$\underline{\phi}_{k+1}^{(q)} = \underline{\phi}_{k+1}^{(q-1)} + \left.\frac{\partial\underline{\phi}}{\partial\underline{i}}\right|_{k+1}^{(q-1)}\cdot\left(\underline{i}_{k+1}^{(q)} - \underline{i}_{k+1}^{(q-1)}\right) \quad (24)$$

- substituting (24) in (23) and collecting $\underline{i}_{k+1}{}^{(q-1)}$ yields:

$$\left(\underline{I} + \frac{2}{\Delta t}\underline{R}^{-1}\cdot\left.\frac{\partial\underline{\phi}}{\partial\underline{i}}\right|_{k+1}^{(q-1)}\right)\underline{i}_{k+1}^{(q)} =$$
$$= -\frac{2}{\Delta t}\underline{R}^{-1}\cdot\left(\underline{\phi}_{k+1}^{(q-1)} - \left.\frac{\partial\underline{\phi}}{\partial\underline{i}}\right|_{k+1}^{(q-1)}\underline{i}_{k+1}^{(q-1)}\right) + \quad (25)$$
$$+\underline{R}^{-1}\cdot\left(\underline{u}_{k+1}+\underline{u}_k\right) - \underline{i}_k + \frac{2}{\Delta t}\underline{R}^{-1}\cdot\underline{\phi}_k$$

with $\underline{I}$ 4×4 identity matrix; finally $\underline{i}_{k+1}{}^{(q-1)}$ is given by:

$$\underline{i}_{k+1}^{(q)} = \left(\underline{R}\frac{\Delta t}{2} + \left.\frac{\partial\underline{\phi}}{\partial\underline{i}}\right|_{k+1}^{(q-1)}\right)^{-1}\cdot$$
$$\cdot\left(\underline{\phi}_k - \underline{\phi}_{k+1}^{(q-1)} + \left.\frac{\partial\underline{\phi}}{\partial\underline{i}}\right|_{k+1}^{(q-1)}\cdot\underline{i}_{k+1}^{(q-1)} + \right. \quad ; \quad (26)$$
$$\left. + \left(\underline{u}_{k+1}+\underline{u}_k\right) - \underline{R}\cdot\underline{i}_k\frac{\Delta t}{2}\right)$$

- the quantities $\underline{\phi}_{k+1}^{(q)}$, $\left.\frac{\partial\underline{\phi}}{\partial\underline{i}}\right|_{k+1}^{(q)}$ can be quickly determined via the method of solution of the magnetic network previously described;
- as starting values (q=0), the following ones are assumed (α value has to be updated from α_k to α_{k+1}):

$$\underline{i}_{k+1}^{(0)} = \underline{i}_k$$
$$\underline{\phi}_{k+1}^{(0)} = \underline{\phi}\left(\underline{i}_{k+1}^{(0)}, \alpha_{k+1}\right) \quad \left.\frac{\partial\underline{\phi}}{\partial\underline{i}}\right|_{k+1}^{(0)} = \frac{\partial\underline{\phi}}{\partial\underline{i}}\left(\underline{i}_{k+1}^{(0)}, \alpha_{k+1}\right) \quad ;(27)$$

- as a stop criterion, the relative value of the ampere-turns variation $\Delta i_{(q)}$ is compared with a predefined threshold value ε_i ($\underline{N}$: diagonal matrix containing the numbers of the winding turns):

$$\Delta i_{(q)} = \frac{\left\|\underline{N}\cdot\underline{i}_{k+1}^{(q)} - \underline{N}\cdot\underline{i}_{k+1}^{(q-1)}\right\|}{\left\|\underline{N}\cdot\underline{i}_{k+1}^{(q)}\right\|} < \varepsilon_i \quad . \quad (28)$$

4. Examples of application

The described technique was applied to the purely hypothetical configuration sketched in Fig.1a, in order to compare the results with the ones obtained by a commercial FEM code for the electromagnetic transient analysis [9]. A time step Δt=50 μs (angular step: $\omega\cdot\Delta t\cdot 180°/\pi$=0.9°) was adopted in the proposed procedure to achieve an adequate angular resolution, while Δt=138.9 μs (angular step: 2.5°) in the FEM transient analysis. Mechanical transient was neglected, assuming a constant rotation speed ω =314.16 s^{-1} (3000 rpm).

A. No-load excitation current build-up

As a first case, the excitation current build-up at no load was considered, starting from null initial value and applying a constant voltage V_e=100 V to the field winding (N_e=1260 turns, R_e=20 Ω). More than 8 s are required to reach a nearly complete steady state running. Figs.5 and 6 show the current i_e and flux linkage ψ_e of the excitation winding, respectively, as functions of time, comparing the results of the proposed procedure and of the FEM transient analysis. The cogging effect on the excitation current is evidenced in Fig.5b. The relative difference is about 3% for the current values, and ≈1.3% with reference to the fluxes.

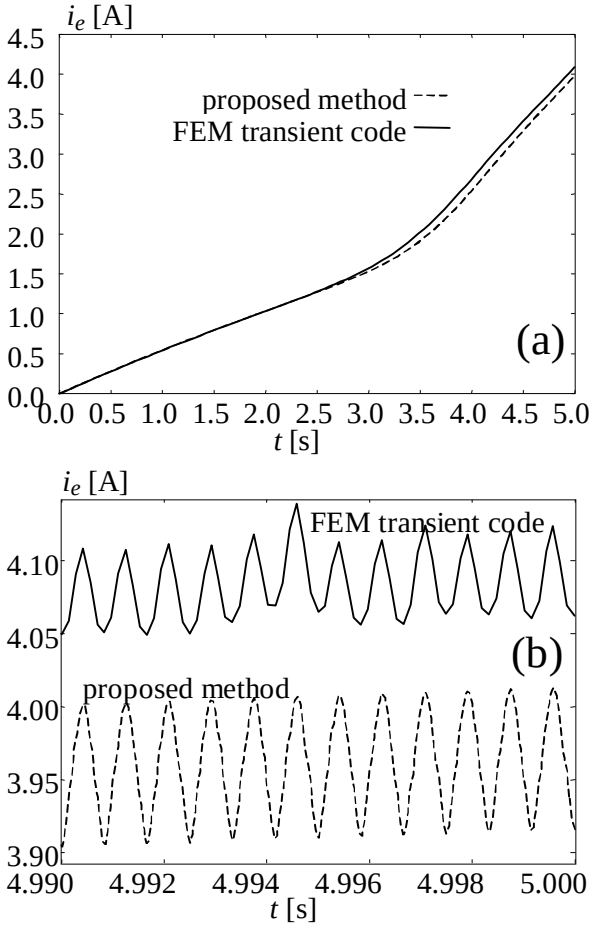

Fig.5. No-load field current i_e: (a) during the entire simulation (with ripple smoothing for sake of clearness); (b) focused on a 10 ms period to display the cogging effect.

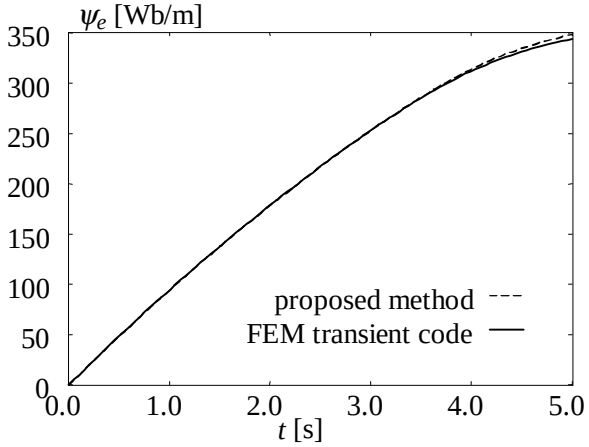

Fig.6: build-up of the excitation flux ψ_e at no-load.

B. Simulation of load insertion

A sudden load insertion (R_a+R_l=3.2 Ω) at t=0 s was simulated maintaining V_e=100 V and assuming initial current values $\{i_1,i_2,i_3,i_e\}$={0,0,0,5 A}. The currents and the flux linkages of the armature windings in the early instants of the transient are compared with the FEM results in Fig.7, showing a good agreement.

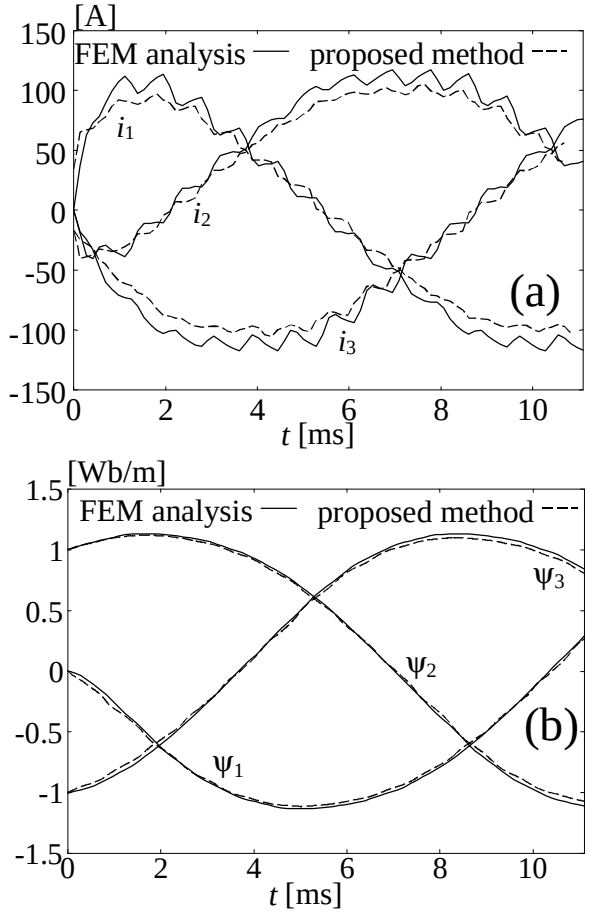

Fig.7: (a) armature currents and (b) flux linkages after a resistive load insertion.

It is worth to remark that the calculation time with the FEM code is at least one order of magnitude higher than that of the proposed method, the same time resolution being maintained.

5. Conclusions

A method for the electromagnetic transient analysis of synchronous machines, based on the solution of an equivalent magnetic circuit, was described. Such method could be extended to a wider class of electromechanical devices with minor modifications of the algorithmic structure.

The examples of application of a code, based on such method, show a good agreement with the results of a commercial FEM code, allowing on the other hand a great reduction of the calculation time.

Acknowledgement

Work financed by the Italian National Ministry of Education, University and Research (MIUR), Cofin 1999, Title: "Electromagnetic Analysis, Modelling and Design Optimisation of Low-Power Synchronous Generators".

References

[1] W. Kunze, H. Kuß, F-Th. Bölter: "Application of Numerical Field Calculation to Selected Problems of Electrical Machines", *Conference SM100*, Zurich, CH, 1991,pp.1193-1198.

[2] J. P. Sturgess, T. W. Preston: "Damper Cage Design Using the Finite-Element Method", *Conference on Electrical Machines and Drives*, Oxford, UK, September 1993, pp.457-462.

[3] T. W. Preston, J. P. Sturgess: "Implementation of the finite-element method into machine design procedures", *6th International Conference on Electrical Machines and Drives*, 1993, pp. 312 – 317.

[4] S.I. Nabeta, A. Foggia, J. L. Coulomb, G. Reyne: "Finite element simulations of unbalanced faults in a synchronous machine", *Transactions on Magnetics, IEEE*, Vol. 32, Issue 3, Part: 1 , May 1996, pp. 1561 – 1564.

[5] E. Schmidt, C. Grabner, G. Traxler-Samek: "Reactance calculation of a 500 MVA hydro-generator using a finite element analysis with superelements ", *Electric Machines and Drives Conference, 2000*, pp. 838 – 844.

[6] E. Schmidt, C. Grabner, G. Traxler-Samek: "Determination of reactances of large hydro-generators using finite elements and domain decomposition ", *Canadian Conference on Electrical and Computer Engineering, 2001*, Vol. 2 , pp. 811 – 817.

[7] V. Ostovich: "Dynamics of Saturated Machines", *Springer Verlag, New York, 1989.*

[8] M. Andriollo, A. Di Gerlando, D. Porzio: "A Design Oriented Magnetic Circuit Model of Low-Power Synchronous Generators", *Proceedings of the 4th International Symposium on Advanced Electromechanical Motion Systems - Electromotion '01*; June 19-20, 2001; Bologna, Italy; pp.535 – 540.

[9] *Ansoft Maxwell 2D Transient Code*, v.8.0.22, 2001.

[10]A. Di Gerlando, R. Perini, I. Vistoli: "A Field-Circuit Approach to the Design Oriented Evaluation of the No-Load Voltage Harmonics of Salient Pole Synchronous Generators"; *Conference Electric Machines and Drives 95*, Durham, UK, September 11-13, 1995; pp.390 – 394.